

Supporting Information

Metallogels: a novel approach for the nanostructuring of single-chain magnets

*Felix Houard,^a Guiseppe Cucinotta,^b Thierry Guizouarn,^a Yan Suffren,^a Guillaume Calvez,^a Carole Daignebonne,^a Olivier Guillou,^a Franck Artzner,^c Matteo Mannini^{*b} and Kevin Bernot^{*ad}*

^a Univ Rennes, INSA Rennes, CNRS, ISCR (Institut des Sciences Chimiques de Rennes), UMR 6226, Université de Rennes 1, F-35000 Rennes, France. E-mail: kevin.bernot@insa-rennes.fr

^b Dipartimento di Chimica "Ugo Schiff" (DICUS), Università degli Studi di Firenze, INSTM Research Unit of Firenze, Via della Lastruccia n.3-13, 50019 Sesto Fiorentino (FI), Italy. E-mail: matteo.mannini@unifi.it

^c CNRS, IPR (Institut de Physique de Rennes), UMR 6251, Université de Rennes 1, F-35000 Rennes, France.

^d Institut Universitaire de France, 1 rue Descartes, 75005, Paris, France.

Materials. Analytical grade solvents (Carlos Elba) and aldehyde (4-octadecyloxy benzaldehyde, TCI Chemicals) were commercially available and used without further purification.

Single crystal X-ray diffraction. Fresh single crystal was mounted on the goniometer head of a D8 Venture (Bruker-AXS) diffractometer equipped with a (CMOS) PHOTON 100 detector [*], using Mo(K α) radiation ($\lambda = 0.71073 \text{ \AA}$, graphite monochromator) at $T = 150(2) \text{ K}$. Crystal structure was solved by dual-space algorithm using SHELXT program,¹ and then refined with full-matrix least-squares methods based on F2 (SHELXL).² All non-hydrogen atoms were refined with anisotropic atomic displacement parameters. H atoms were finally included in their calculated positions and treated as riding on their parent atom with constrained thermal parameters. Supplementary crystallographic data can be obtained free of charge from the Cambridge Crystallographic Data Centre (CCDC) under the deposition numbers CCDC-2178278 (NITPhOC₁₈).

Powder X-ray diffraction. Experimental diffraction patterns have been collected with a Panalytical X'pert Pro diffractometer, equipped with an X'Celerator detector. Typical recording conditions were 45 kV, 40 mA for Cu(K α) ($\lambda = 1.542 \text{ \AA}$) in θ/θ mode. Calculated patterns from single-crystal measurements were simulated using the Mercury program from CCDC.

Fourier Transformed Infra-Red spectroscopy. FT-IR studies were performed with a Perkin Elmer Frontier UATR spectrometer on as-synthesized powders, gels and xerogels (from 4000 to 650 cm^{-1} , res. 1 cm^{-1}).

Variable temperature UV-Visible spectroscopy. UV-Visible absorption spectra of solutions and gels were recorded with a Jasco-V670 spectrometer (from 800 to 450 nm, 400 $\text{nm}\cdot\text{min}^{-1}$, res. 1 nm) in 1 mm Hellma 110-QS cuvettes.

Elemental analyses. Elemental analyses (CHNS) were realized with a Thermo Fischer FlashEA 1112 analyser.

Electron Spin Resonance (ESR) spectroscopy. Fresh solution and gel samples were prepared inside quartz tubes. ESR spectra were recorded on a Bruker EMX-8/2.7 (X-band) spectrometer at room temperature.

Small Angle X-ray Scattering (SAXS) and fiber diffraction. Fresh gel samples were prepared inside quartz capillaries. SAXS experiments were performed at room temperature with an home-made setup, using X-ray patterns collected with a Pilatus 300K (Dectris, Grenoble, France) mounted on a GeniX 3D (Xenocs, Sassenage, France) microsource X-ray generator operating at 30 W with a monochromatic Cu(K α) radiation is of $\lambda = 1.541 \text{ \AA}$. The sample-to-detector distance is 270 mm, and the diffraction patterns were recorded for reciprocal spacing $q = 4\pi \times \sin(\theta)/\lambda$ in a range of repetitive distances from 0.01 \AA^{-1} (600 \AA) to 1.77 \AA^{-1} (8 \AA). Images were transformed into graphics using a home-developed program.

Magnetic studies. Magnetic studies were performed using an MPMS SQUID magnetometer equipped with an RSO probe and a ^3He insert for hysteresis measurements below 1.5 K (field sweep rate was 15.5 $\text{Oe}\cdot\text{s}^{-1}$). Ground powder of xerogels was pressed into pellets to avoid in-field crystallite orientation. Fresh gels were transferred in gelatin capsules and quickly frozen at 100 K (the freezing point of the *n*-heptane being 182 K) to avoid further degradations. Powder measurements were corrected from diamagnetic contributions as calculated with Pascal's constants, and the gel ones by subtracting the diamagnetic contributions of the capsule and solvent measured in the same conditions.

Atomic Force Microscopy. AFM studies were performed on cleaned silicon substrates (Si <100>, n-doped, 2-5 Ω -cm, Virginia Semiconductors) on which 10 μ L of gel solutions were dropped and spin-coated at 2000 rpm for 60 seconds. Fresh samples then were kept at 4°C for 2 min, dried under a dry N₂ flux for 15 seconds and mounted on the AFM sample holder. Samples were measured in semicontact mode at room temperature under a gentle nitrogen anhydrous flux to avoid deterioration of the soft film, with an SPM Solver P47 Pro (NT-MDT Spectrum Instrument) and HQ:NSC36/Al BS silicon tips (cantilever B, 130 kHz, 2 N·m⁻¹, MikroMasch). Results and imaging were processed with Gwyddion v2.56 software,³ raw images have been treated with an horizontal line by line subtraction using a “median of differences” routine in order to fix the line scan misalignment issue.

Gelation inversion test. Gelation properties were evaluated by introducing a precise amount of the targeted compound and a volume of solvent needed to reach the required weight concentration. The vial was closed and heated with a heat gun until complete dissolution of the compound and homogenization of the solution. The solution was quickly cooled at 4°C for several minutes to hours, depending on the gelling dynamics of the compound and the concentration. The effective gelation of the sample was tested by inverting the vial: if the gel does not flow after one minute, then the test is positive.

Synthesis and gelation properties

Synthesis of the nitronyl-nitroxide radical, NITPhOC₁₈

2-(4'-(octadecyloxy)phenyl)-4,4,5,5-tetramethylimidazolin-1-oxyl-3-oxide

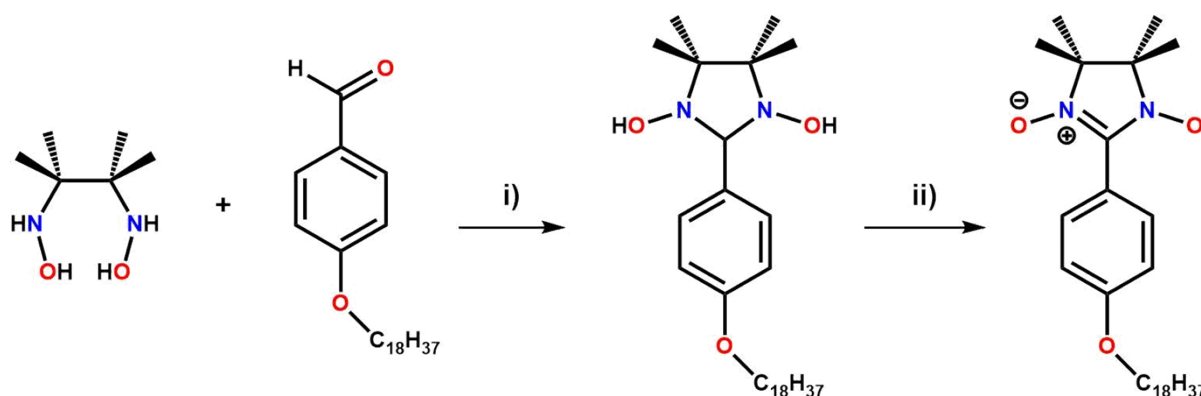


Fig. S1. Synthetic pathway for the preparation of NITPhOC₁₈: i) MeOH, 25°C, 3 days; iii) NaIO₄, CH₂Cl₂:H₂O.

2.5 mmol (936 mg, 1 eq.) of commercially available 4-(octadecyloxy)benzaldehyde was added to 5 mmol (741 mg, 2 eq.) of 2,3-bis(hydroxylamino)-2,3-dimethylbutane in 50 mL of methanol, and stirred at room temperature for three days. The solution was dried and the remaining milky-white waxy solid was dissolved in 50 mL of cold CH_2Cl_2 , then 50 mL of a NaIO_4 aqueous solution (641.6 mg, 3 mmol, 1.5 eq.) was added. The mixture immediately turned dark blue, the organic phase was washed several times with water (3 x 100 mL) and separated. The resultant organic solution was dried on Na_2SO_4 , concentrated under reduced pressure and purified by flash silica gel (40-60 μm , 60 Å) column chromatography eluted with a 3/1 (v/v) ether/*n*-pentane solution. A dark blue fraction was collected and concentrated under reduced pressure, resulting in 313.6 mg (0.625 mmol) of fine blue crystalline solid. Yield: 25%. Single crystals suitable for single-crystal XRD were obtained by slow inter diffusion of 0.05 mmol (25.5 mg) of NITPhOC_{18} in 7 mL of CH_2Cl_2 layered with 10 mL of *n*-heptane, kept at 4°C. Single crystals were isolated after few days. Elemental analysis (%) calcd. for $\text{C}_{31}\text{H}_{53}\text{N}_2\text{O}_3$: C 74.20, H 10.65, N 5.58. Found: C 74.55, H 10.51, N 5.54.

Synthesis of precursor, $[\text{Tb}(\text{hfac})_3 \cdot \text{NITPhOC}_{18}]_{\infty}$

0.1 mmol (1 eq., 81.6 mg) of $[\text{Tb}(\text{hfac})_3 \cdot 2\text{H}_2\text{O}]$ was dissolved in 40 mL of dry boiling *n*-heptane. The solution was concentrated until the volume reaches 10 mL, then cooled to 75°C. 0.1 mmol (1 eq., 50.1 mg) of NITPhOC_{18} dissolved in 3 mL of CHCl_3 was slowly added under stirring, and the final mixture was dried under reduced pressure at room temperature, giving a dark green latex-like solid. Yield: 65%. Elemental analysis (%) calcd. for $\text{TbC}_{46}\text{H}_{56}\text{N}_2\text{O}_9\text{F}_{18}$: C 43.10, H 4.40, N 2.19. Found: C 42.84, H 4.21, N 2.32.

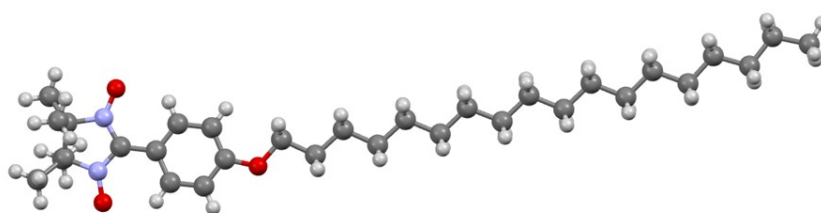
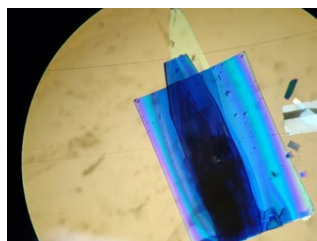


Fig. S2. Crystals of NITPhOC_{18} observed under optical microscope (x63 magnification, left) and structural representations of the NITPhOC_{18} (right).

Table S1. Crystallographic parameters of NITPhOC₁₈.

M_w (g·mol⁻¹)	501.75
Crystal system	Monoclinic
Space group	P2 ₁ /n (N°14)
a (Å)	7.4068(13)
b (Å)	44.744(8)
c (Å)	8.8243(17)
α [°]	90
β [°]	94.435(7)
γ [°]	90
V [Å³]	2915.7(9)
Z	4
T (K)	150(2)
2θ range	2.359 - 25.680
Refins collected	9894
Indep. reflns	5236
Obs. reflns	3825
Parameters	332
R_1 [$I > 2\sigma(I)$]^{a)} / wR_2 [$I > 2\sigma(I)$]^{b)}	12.40 / 33.23
GOF	1.079

$$a) \sum (|F_0| - |F_c|) / \sum |F_0|$$

$$b) \sqrt{\sum w(|F_0|^2 - |F_c|^2)^2 / \sum w(|F_0|^2)^2}$$

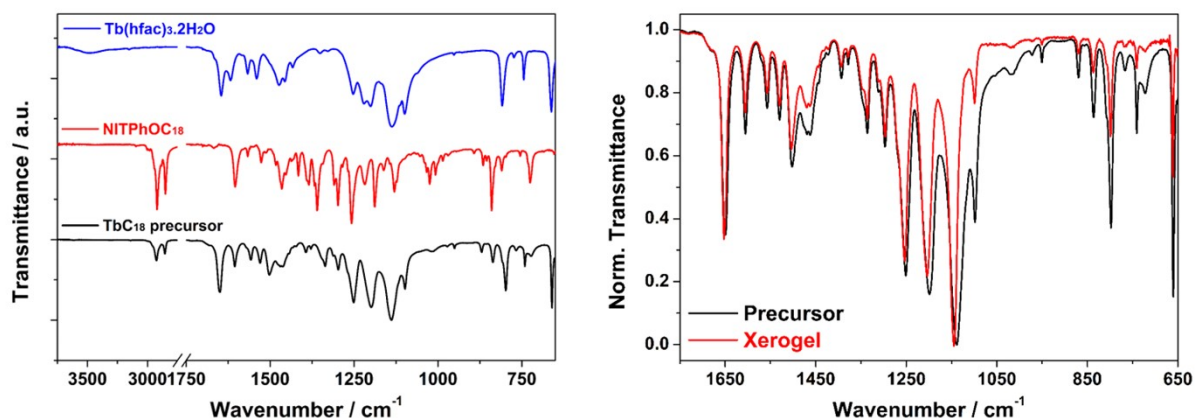


Fig. S3. Comparative FT-IR spectra between $[\text{Tb}(\text{hfac})_3 \cdot 2\text{H}_2\text{O}]$, NITPhOC_{18} and the TbC_{18} precursor (left) and between the TbC_{18} precursor and the TbC_{18} xerogel (right).

$[\text{Tb}(\text{hfac})_3 \cdot 2\text{H}_2\text{O}]$: 3482 cm^{-1} , 1646 cm^{-1} , 1618 cm^{-1} , 1567 cm^{-1} , 1540 cm^{-1} , 1473 cm^{-1} , 1456 cm^{-1} , 1433 cm^{-1} , 1252 cm^{-1} , 1220 cm^{-1} , 1201 cm^{-1} , 1137 cm^{-1} , 1099 cm^{-1} , 809 cm^{-1} , 744 cm^{-1} , 662 cm^{-1} .

$[\text{NITPhOC}_{18}]$: 2921 cm^{-1} , 2851 cm^{-1} , 1604 cm^{-1} , 1526 cm^{-1} , 1465 cm^{-1} , 1416 cm^{-1} , 1384 cm^{-1} , 1360 cm^{-1} , 1298 cm^{-1} , 1257 cm^{-1} , 1218 cm^{-1} , 1188 cm^{-1} , 1130 cm^{-1} , 1025 cm^{-1} , 840 cm^{-1} , 725 cm^{-1} .

$[\text{TbC}_{18}$ precursor]: 2925 cm^{-1} , 2855 cm^{-1} , 1649 cm^{-1} , 1605 cm^{-1} , 1557 cm^{-1} , 1530 cm^{-1} , 1502 cm^{-1} , 1336 cm^{-1} , 1297 cm^{-1} , 1251 cm^{-1} , 1199 cm^{-1} , 1138 cm^{-1} , 1098 cm^{-1} , 870 cm^{-1} , 836 cm^{-1} , 798 cm^{-1} , 741 cm^{-1} , 660 cm^{-1} .

$[\text{TbC}_{18}$ xerogel]: 2926 cm^{-1} , 2855 cm^{-1} , 1653 cm^{-1} , 1605 cm^{-1} , 1557 cm^{-1} , 1530 cm^{-1} , 1504 cm^{-1} , 1336 cm^{-1} , 1296 cm^{-1} , 1253 cm^{-1} , 1204 cm^{-1} , 1145 cm^{-1} , 1099 cm^{-1} , 870 cm^{-1} , 837 cm^{-1} , 798 cm^{-1} , 741 cm^{-1} , 661 cm^{-1} .

Table S2. Minimum gelation concentration (C_{MG}) in $\text{mg}\cdot\text{mL}^{-1}$ of TbC_{18} gel (S = Solution, I = Insoluble).

Solvent	C_{MG} ($\text{mg}\cdot\text{mL}^{-1}$)
<i>n</i> -hexane	10
<i>n</i> -heptane	8
<i>n</i> -octane	8
<i>n</i> -decane	5
Cyclohexane	S
Xylenes	S
Toluene	S
Ether	S
Chloroform, DCM	S
Acetone	S
Acetonitrile	S
Methanol, Ethanol	S
Water	I

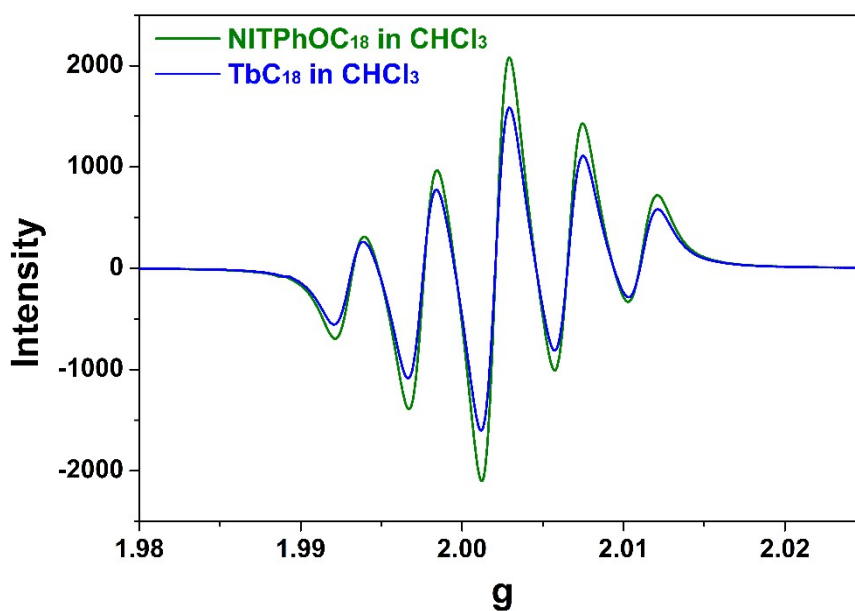


Fig. S4. EPR spectra of CHCl_3 solutions of NITPhOC_{18} ($C_m = 3.9 \text{ mg}\cdot\text{mL}^{-1}$) and TbC_{18} precursor ($C_m = 10 \text{ mg}\cdot\text{mL}^{-1}$).

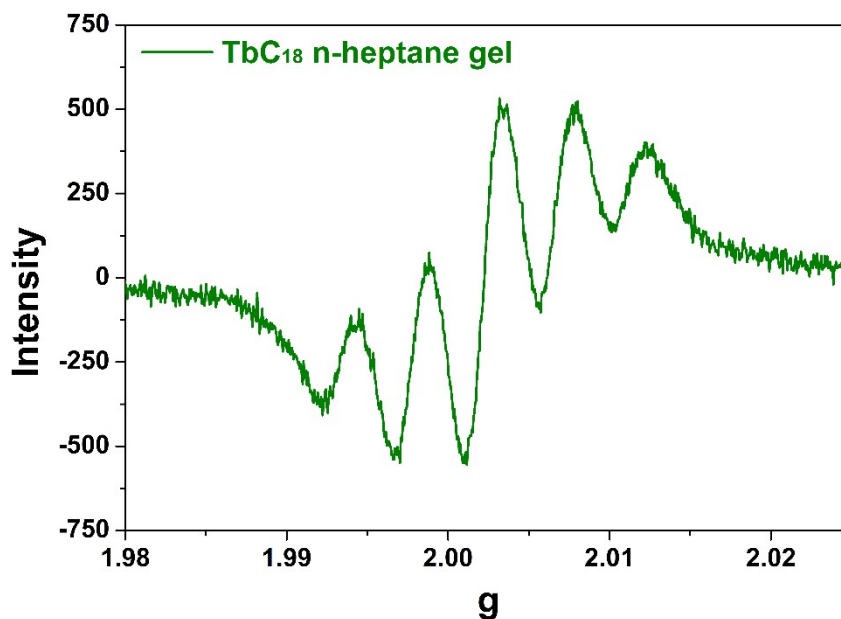


Fig. S5. Zoom of the EPR spectrum of the *n*-heptane TbC₁₈ gel ($C_m = 10 \text{ mg}\cdot\text{mL}^{-1}$).

Table S3. EPR extracted g_e and hyperfine coupling a_n values for CHCl₃ solutions of NITPhOC₁₈ and TbC₁₈, and *n*-heptane TbC₁₈ gel.

NITPhOC ₁₈ solution (3.9 mg·mL ⁻¹ , CHCl ₃) ^{a)}		TbC ₁₈ solution (10 mg·mL ⁻¹ , CHCl ₃)		TbC ₁₈ gel (10 mg·mL ⁻¹ , <i>n</i> -heptane)	
g_e	a_n (mT)	g_e	a_n (mT)	g_e	a_n (mT)
2.0071	0.76	2.0071	0.77	2.0073	0.76

a) In order to compare the NITPhOC₁₈ and the TbC₁₈ at the same molar concentration ($C = 7.81 \mu\text{mol}\cdot\text{mL}^{-1}$).

Morphology and structural model

In order to have a complete representation, we have decided to build a simple 3D structural model of these nanotubes. Because they are made of helical chains, we based our model on the parametric equations (whose parameter is t) of the helix below (Equation S1) to calculate the relative position of each Tb^{III} atom.

$$\begin{cases} x(t) = r_0 \cdot \cos\left(\frac{2\pi}{N} \cdot i\right) \\ y(t) = r_0 \cdot \theta \cdot \sin\left(\frac{2\pi}{N} \cdot i\right) \\ z(t) = \frac{h}{2\pi} \cdot t \end{cases} \quad \text{Eq.S1}$$

with r_0 being the tube radius, θ the direction of rotation of the helix ($\theta = +1$ for anticlockwise, $\theta = -1$ for clockwise) and h the pitch of the helix.

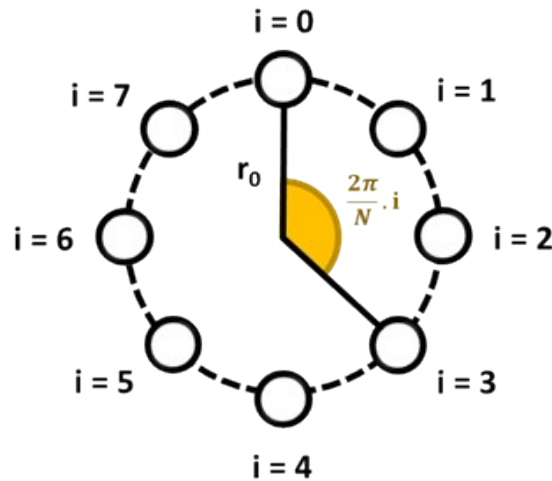


Fig. S6. Schematic representation of the determination of “shift” φ between consecutive chains.

Our nanotube is constituted of a periodic arrangement of eight helices, so we had to introduce a “shift” between the helices on the unit circle of radius r_0 , by adding the equivalent of a “phase difference” φ to the trigonometric terms:

$$\begin{cases} x_i(t) = r_0 \cdot \cos(t + \varphi_i) \\ y_i(t) = r_0 \cdot \theta \cdot \sin(t + \varphi_i) \\ z(t) = \frac{h}{2\pi} \cdot t \end{cases} \quad \text{Eq.S2}$$

with $\varphi_i = 2\pi \cdot i/N$, i being the helix' number and N the total number of helices.

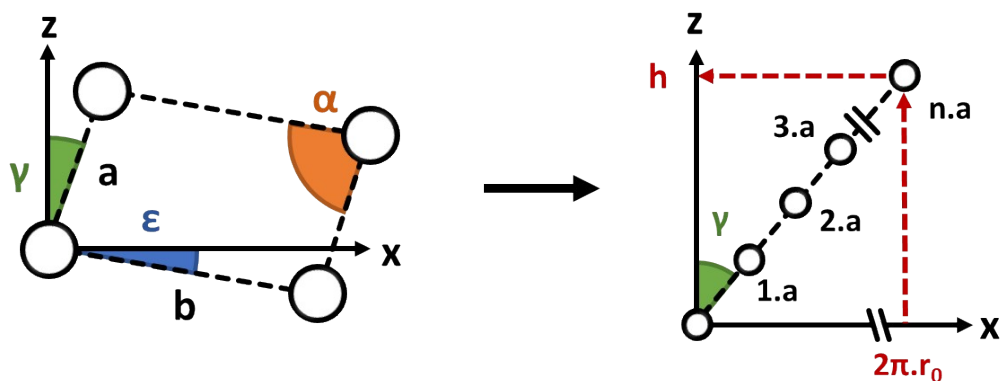


Fig. S7. Schematic representation of the determination of the value of the pitch h .

Then, the pitch length h can be easily estimated from the 2D monoclinic parameters: it is equivalent to a projection of $n \cdot a$ segments on the unit circle (or the x -axis in Fig. S7 above), which have to be at least equal to at a complete revolution $2\pi \cdot r_0$. By using the right-angled triangle ratios, we obtain:

$$\tan(\pi - \gamma) = \frac{h}{2\pi \cdot r_0} \quad \text{Eq.S3}$$

$$h = 2\pi \cdot r_0 \cdot \tan(\pi - \gamma) \quad \text{Eq.S4}$$

An additional difficulty is that the neighboring chains do not strictly face each other's but are slightly tilted by an angle $\epsilon = 8^\circ$. We have to determine then the initial position of the first atoms of each chain along the tube axis z , *i.e.*, the shift of each helix.

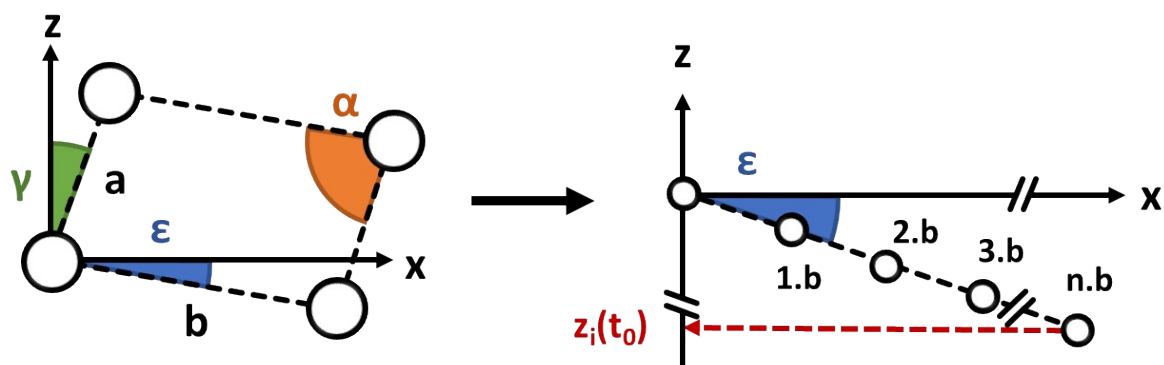


Fig. S8. Schematic representation of the determination of the relative z position of each atom.

Once again, this value is given by a simple trigonometric relation and can be generalized thanks to the periodicity of the system:

$$z_i(t_0) = b \cdot \sin(\varepsilon) \cdot i \quad \text{Eq.S5}$$

The periodic interval between two consecutive intrachain Tb^{III} atoms along z is also given by the following relation:

$$z_i(t_{n+1}) = a \cdot \cos(\gamma) \quad \text{Eq.S6}$$

Then, for any helix, the position according to the z-axis of the nth atom of the chain will be:

$$z_i(t_n) = n \cdot z_i(t_{n+1}) + z_i(t_0) \quad \text{Eq.S7}$$

$$z_i(t_n) = n \cdot a \cdot \cos(\gamma) + b \cdot \sin(\varepsilon) \cdot i \quad \text{Eq.S8}$$

The parameter t , linked to the $z(t)$ position of each atom, is then determined by combining Eq. S1 and S8.

$$z_i(t_n) = \frac{h}{2\pi} \cdot t_n = n \cdot a \cdot \cos(\gamma) + b \cdot \sin(\varepsilon) \cdot i \quad \text{Eq.S9}$$

$$t_n = \frac{2\pi}{h} \cdot (n \cdot a \cdot \cos(\gamma) + b \cdot \sin(\varepsilon) \cdot i) \quad \text{Eq.S10}$$

These t parameters are finally implemented in the $x(t)$ and $y(t)$ equations from Eq. S2 to obtain the coordinates. The resulting model is depicted in Fig. 4e, and the relative atom positions are reported in Table S4 below.

Table S4. Relative positions of the Tb^{III} atoms* of a nanotube reconstructed from the structural model proposed, within a virtual unit cell of parameters $a = b = 36 \text{ \AA}$, $c = 477.00 \text{ \AA}$, $\alpha = \beta = \gamma = 90^\circ$.

Helix n°1			Helix n°2			Helix n°3			Helix n°4		
x(t)	y(t)	z(t)									
1.000	0.500	0.027	0.869	0.838	0.024	0.544	0.998	0.020	0.196	0.897	0.016
0.992	0.591	0.044	0.802	0.899	0.040	0.453	0.998	0.036	0.129	0.836	0.032
0.967	0.678	0.060	0.724	0.947	0.056	0.364	0.981	0.052	0.075	0.763	0.048
0.927	0.760	0.076	0.640	0.980	0.072	0.279	0.948	0.068	0.034	0.682	0.064
0.873	0.833	0.092	0.550	0.997	0.088	0.201	0.901	0.084	0.009	0.594	0.080
0.807	0.895	0.108	0.460	0.998	0.105	0.134	0.840	0.101	0.000	0.504	0.097
0.730	0.944	0.125	0.370	0.983	0.121	0.078	0.768	0.117	0.008	0.413	0.113
0.646	0.978	0.141	0.285	0.951	0.137	0.036	0.687	0.133	0.032	0.325	0.129
0.557	0.997	0.157	0.206	0.905	0.153	0.010	0.600	0.149	0.071	0.243	0.145
0.466	0.999	0.173	0.138	0.845	0.169	0.000	0.510	0.165	0.124	0.170	0.161
0.376	0.984	0.189	0.082	0.774	0.185	0.007	0.419	0.182	0.190	0.107	0.178
0.290	0.954	0.206	0.039	0.693	0.202	0.029	0.331	0.198	0.267	0.058	0.194
0.212	0.908	0.222	0.011	0.607	0.218	0.068	0.249	0.214	0.351	0.023	0.210
0.142	0.849	0.238	0.000	0.516	0.234	0.120	0.175	0.230	0.440	0.004	0.226
0.085	0.779	0.254	0.006	0.426	0.250	0.186	0.111	0.246	0.530	0.001	0.242
0.041	0.699	0.270	0.027	0.337	0.266	0.261	0.061	0.262	0.620	0.015	0.259
0.013	0.613	0.287	0.065	0.254	0.283	0.345	0.025	0.279	0.706	0.045	0.275
0.001	0.523	0.303	0.116	0.180	0.299	0.433	0.004	0.295	0.785	0.089	0.291
0.005	0.432	0.319	0.181	0.115	0.315	0.524	0.001	0.311	0.855	0.148	0.307
0.025	0.343	0.335	0.256	0.064	0.331	0.614	0.013	0.327	0.913	0.218	0.323
0.061	0.260	0.351	0.339	0.027	0.347	0.700	0.042	0.343	0.957	0.297	0.340
0.112	0.184	0.367	0.427	0.005	0.364	0.780	0.086	0.360	0.986	0.384	0.356
0.176	0.119	0.384	0.518	0.000	0.380	0.850	0.143	0.376	0.999	0.474	0.372
0.250	0.067	0.400	0.608	0.012	0.396	0.909	0.213	0.392	0.996	0.564	0.388
0.333	0.029	0.416	0.695	0.039	0.412	0.955	0.292	0.408	0.976	0.653	0.404
0.421	0.006	0.432	0.775	0.082	0.428	0.985	0.377	0.424	0.940	0.737	0.420
0.511	0.000	0.448	0.846	0.139	0.445	0.999	0.467	0.441	0.890	0.813	0.437
0.602	0.010	0.465	0.906	0.208	0.461	0.997	0.558	0.457	0.827	0.878	0.453
0.689	0.037	0.481	0.952	0.286	0.477	0.978	0.647	0.473	0.753	0.931	0.469
0.769	0.079	0.497	0.983	0.371	0.493	0.943	0.731	0.489	0.671	0.970	0.485
0.841	0.135	0.513	0.998	0.461	0.509	0.894	0.808	0.505	0.583	0.993	0.501
0.902	0.202	0.529	0.997	0.552	0.525	0.832	0.874	0.522	0.492	1.000	0.518
0.949	0.280	0.546	0.980	0.641	0.542	0.759	0.928	0.538	0.402	0.990	0.534
0.981	0.365	0.562	0.946	0.726	0.558	0.677	0.968	0.554	0.315	0.964	0.550
0.998	0.455	0.578	0.898	0.803	0.574	0.589	0.992	0.570	0.234	0.923	0.566

* These data can be found as supplementary material as a .xyz and .mryx (Mercury 2021.2.0 software from CCDC)

**The c parameter value has been fixed arbitrarily.

Helix n°5			Helix n°6			Helix n°7			Helix n°8		
x(t)	y(t)	z(t)	x(t)	x(t)	y(t)	z(t)	x(t)	x(t)	y(t)	z(t)	x(t)
0.008	0.588	0.012	0.078	0.008	0.588	0.012	0.078	0.008	0.588	0.012	0.078
0.000	0.497	0.028	0.133	0.000	0.497	0.028	0.133	0.000	0.497	0.028	0.133
0.009	0.407	0.044	0.201	0.009	0.407	0.044	0.201	0.009	0.407	0.044	0.201
0.034	0.319	0.060	0.278	0.034	0.319	0.060	0.278	0.034	0.319	0.060	0.278
0.074	0.238	0.077	0.363	0.074	0.238	0.077	0.363	0.074	0.238	0.077	0.363
0.129	0.165	0.093	0.452	0.129	0.165	0.093	0.452	0.129	0.165	0.093	0.452
0.196	0.103	0.109	0.543	0.196	0.103	0.109	0.543	0.196	0.103	0.109	0.543
0.272	0.055	0.125	0.633	0.272	0.055	0.125	0.633	0.272	0.055	0.125	0.633
0.357	0.021	0.141	0.718	0.357	0.021	0.141	0.718	0.357	0.021	0.141	0.718
0.446	0.003	0.157	0.796	0.446	0.003	0.157	0.796	0.446	0.003	0.157	0.796
0.537	0.001	0.174	0.864	0.537	0.001	0.174	0.864	0.537	0.001	0.174	0.864
0.627	0.016	0.190	0.920	0.627	0.016	0.190	0.920	0.627	0.016	0.190	0.920
0.712	0.047	0.206	0.962	0.712	0.047	0.206	0.962	0.712	0.047	0.206	0.962
0.791	0.093	0.222	0.989	0.791	0.093	0.222	0.989	0.791	0.093	0.222	0.989
0.859	0.152	0.238	1.000	0.859	0.152	0.238	1.000	0.859	0.152	0.238	1.000
0.916	0.223	0.255	0.994	0.916	0.223	0.255	0.994	0.916	0.223	0.255	0.994
0.960	0.303	0.271	0.972	0.960	0.303	0.271	0.972	0.960	0.303	0.271	0.972
0.988	0.390	0.287	0.934	0.988	0.390	0.287	0.934	0.988	0.390	0.287	0.934
1.000	0.480	0.303	0.882	1.000	0.480	0.303	0.882	1.000	0.480	0.303	0.882
0.995	0.571	0.319	0.817	0.995	0.571	0.319	0.817	0.995	0.571	0.319	0.817
0.974	0.659	0.336	0.742	0.974	0.659	0.336	0.742	0.974	0.659	0.336	0.742
0.937	0.742	0.352	0.659	0.937	0.742	0.352	0.659	0.937	0.742	0.352	0.659
0.886	0.818	0.368	0.570	0.886	0.818	0.368	0.570	0.886	0.818	0.368	0.570
0.822	0.882	0.384	0.480	0.822	0.882	0.384	0.480	0.822	0.882	0.384	0.480
0.748	0.934	0.400	0.389	0.748	0.934	0.400	0.389	0.748	0.934	0.400	0.389
0.665	0.972	0.417	0.303	0.665	0.972	0.417	0.303	0.665	0.972	0.417	0.303
0.577	0.994	0.433	0.223	0.577	0.994	0.433	0.223	0.577	0.994	0.433	0.223
0.486	1.000	0.449	0.152	0.486	1.000	0.449	0.152	0.486	1.000	0.449	0.152
0.396	0.989	0.465	0.093	0.396	0.989	0.465	0.093	0.396	0.989	0.465	0.093
0.309	0.962	0.481	0.047	0.309	0.962	0.481	0.047	0.309	0.962	0.481	0.047
0.228	0.920	0.498	0.016	0.228	0.920	0.498	0.016	0.228	0.920	0.498	0.016
0.157	0.864	0.514	0.001	0.157	0.864	0.514	0.001	0.157	0.864	0.514	0.001
0.097	0.795	0.530	0.003	0.097	0.795	0.530	0.003	0.097	0.795	0.530	0.003
0.050	0.717	0.546	0.021	0.050	0.717	0.546	0.021	0.050	0.717	0.546	0.021
0.018	0.632	0.562	0.055	0.018	0.632	0.562	0.055	0.018	0.632	0.562	0.055

Magnetic properties

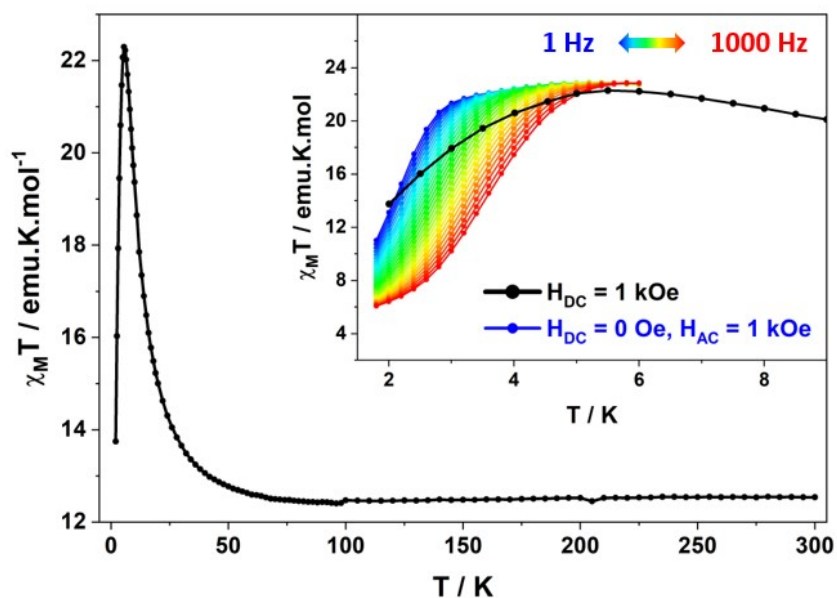


Fig. S9. Temperature dependence of $\chi_M T$ product for TbC₁₈ xerogel measured with $H_{DC} = 1000 \text{ Oe}$ and with inset, a zoom in the low-temperature region with the $\chi_M T$ product reconstructed from AC measurements with $H_{AC} = 3 \text{ Oe}$ at different frequencies.

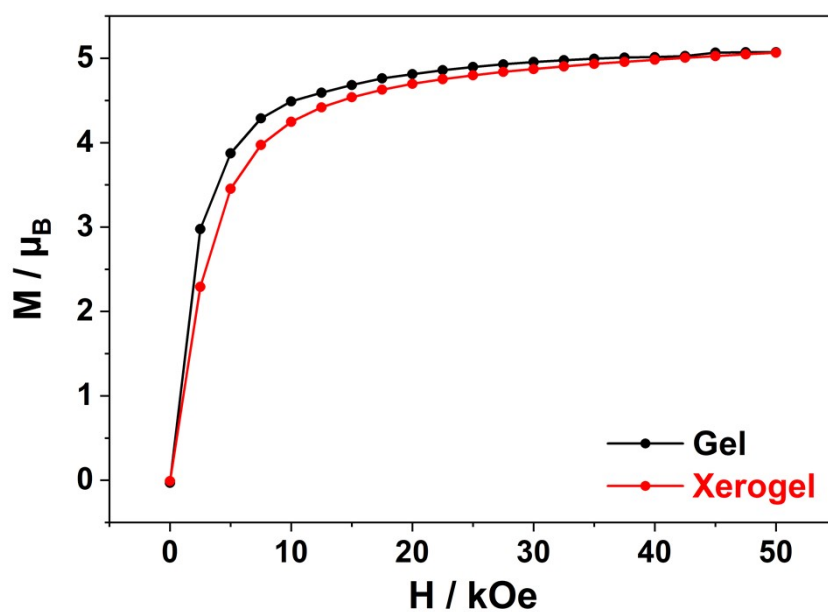


Fig. S10. Field dependence of magnetization at 2K of *n*-heptane TbC₁₈ gel ($C_m = 10 \text{ mg}\cdot\text{mL}^{-1}$) and xerogel.

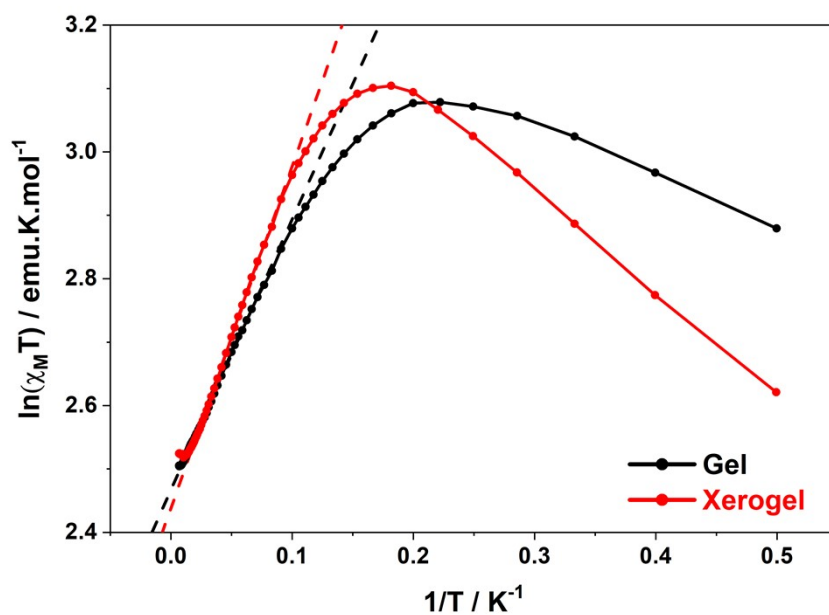


Fig. S11. Reciprocal temperature dependence of $\ln(\chi_M T)$ of *n*-heptane TbC_{18} gel ($C_m = 10 \text{ mg}\cdot\text{mL}^{-1}$) and xerogel, with best fit as a dashed line.

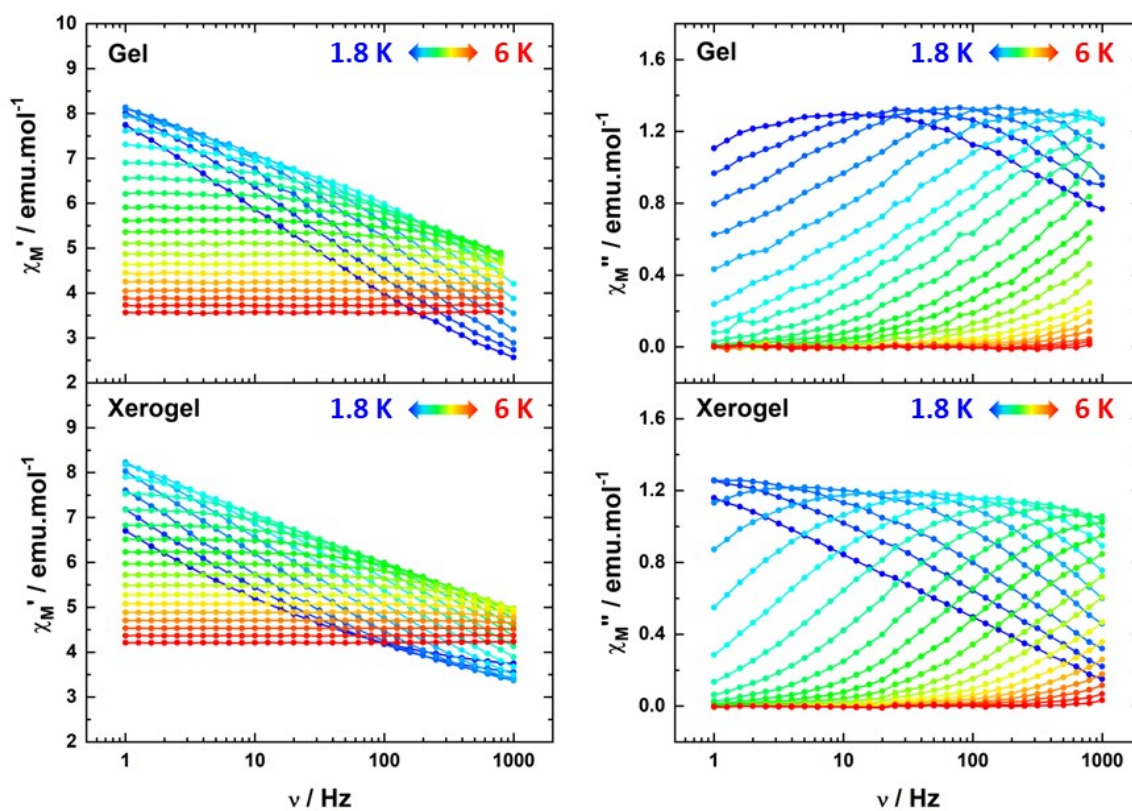


Fig. S12. Frequency dependence of the in-phase (χ_M' , left) and out-of-phase (χ_M'' , right) susceptibilities of *n*-heptane TbC_{18} gel ($C_m = 10 \text{ mg}\cdot\text{mL}^{-1}$) and xerogel in zero external dc field.

Table S5. Relaxation times extracted in zero external dc field for *n*-heptane TbC₁₈ gel ($C_m = 10 \text{ mg}\cdot\text{mL}^{-1}$) and xerogel.

Gel			Xerogel		
T (K)	τ (μs)	R^2	T (K)	τ (μs)	R^2
1.8	14752	0.9971	1.8	216877	0.9933
2.0	5854	0.9904	2.0	115846	0.9919
2.2	2708	0.9849	2.2	64185	0.887
2.4	1012	0.9891	2.4	25662	0.9817
2.6	406	0.9976	2.6	9020	0.9783
2.8	226	0.9990	2.8	3289	0.9863
3.0	136	0.9982	3.0	1464	0.9849
			3.2	797	0.9872
			3.4	508	0.9908
			3.6	343	0.9932
			3.8	255	0.9950
			4.0	198	0.9966

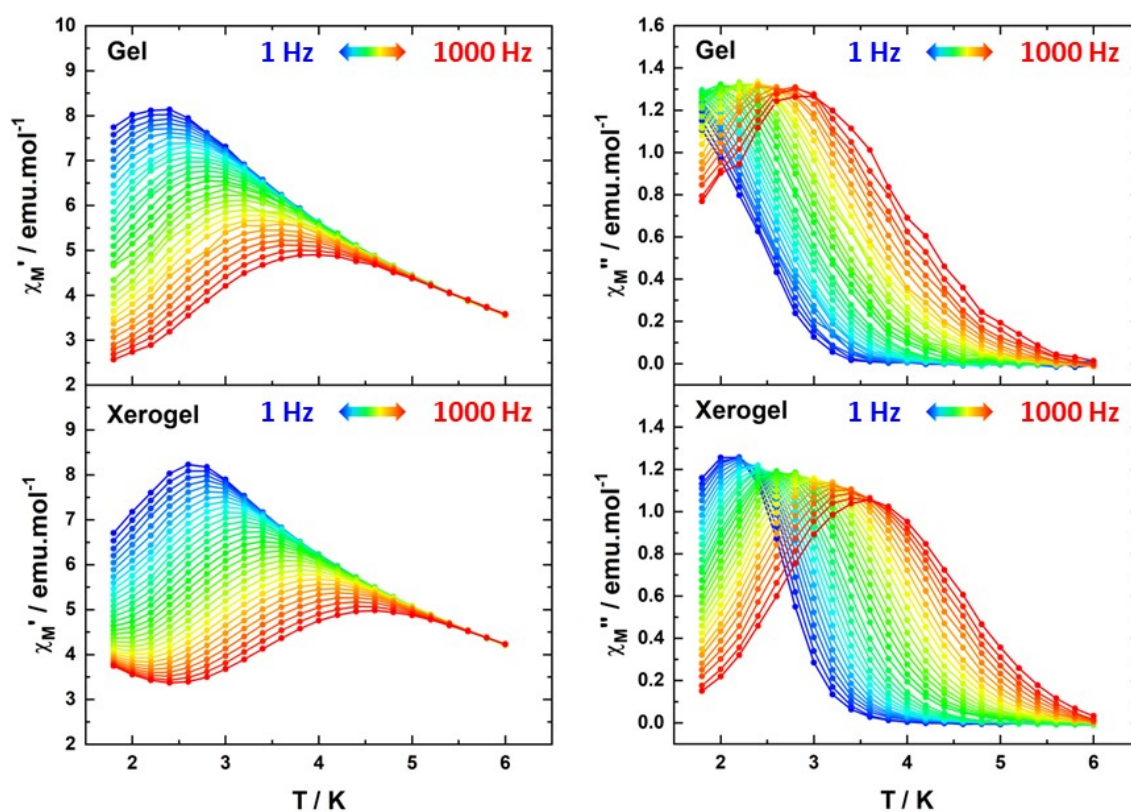


Fig. S13. Temperature dependency of the in-phase (χ_M' , left) and out-of-phase (χ_M'' , right) susceptibilities of *n*-heptane TbC₁₈ gel ($C_m = 10 \text{ mg}\cdot\text{mL}^{-1}$) and xerogel in zero external dc field.

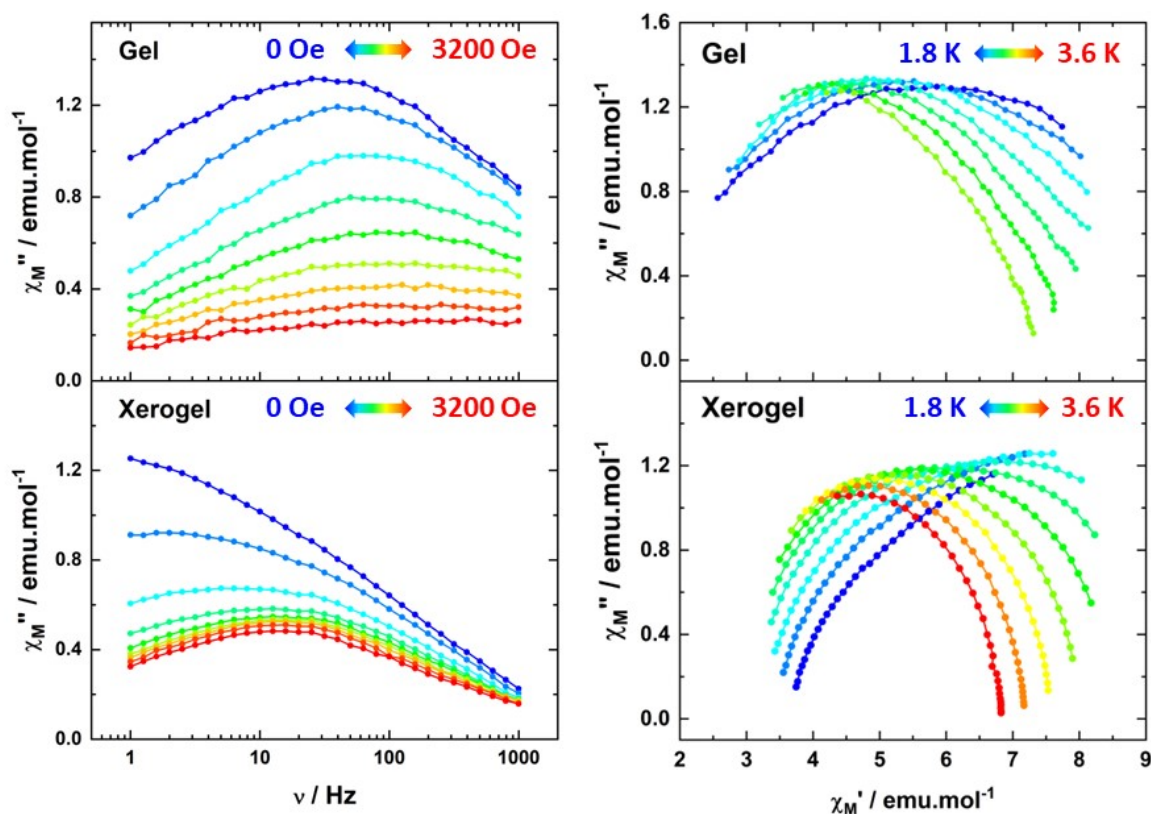


Fig. S14. Field dependency of out-of-phase (χ_M'') susceptibilities at 2 K for *n*-heptane TbC_{18} gel ($C_m = 10 \text{ mg}\cdot\text{mL}^{-1}$, top left) and xerogel (bottom left) and Cole-Cole diagrams in zero external dc field at different temperatures for *n*-heptane TbC_{18} gel ($C_m = 10 \text{ mg}\cdot\text{mL}^{-1}$, top right) and xerogel (bottom right).

Table S6. Adiabatic (χ_s), isothermal (χ_T) susceptibility values and relaxation times distribution (α) extracted in zero external dc field for *n*-heptane TbC_{18} gel ($C_m = 10 \text{ mg}\cdot\text{mL}^{-1}$) and xerogel.

Gel					Xerogel				
T (K)	χ_s	χ_T	α	R^2	T (K)	χ_s	χ_T	α	R^2
1.8	0.83	10.81	0.675	0.9970	1.8	3.09	9.58	0.611	0.9943
2.0	0.75	10.18	0.653	0.9915	2.0	2.80	9.74	0.610	0.9927
2.2	0.13	10.02	0.669	0.9929	2.2	2.51	9.86	0.621	0.990
2.4	0.4	9.20	0.633	0.9943	2.4	2.19	9.64	0.628	0.9840
2.6	0.63	8.48	0.590	0.9937	2.6	1.98	9.01	0.616	0.9819
2.8	0.99	7.90	0.547	0.9933	2.8	1.93	8.22	0.580	0.9899
3.0	1.23	7.42	0.510	0.9938	3.0	2.03	7.53	0.529	0.9866
					3.2	2.23	6.98	0.469	0.9869
					3.4	2.50	6.55	0.406	0.9892
					3.6	2.74	6.19	0.350	0.9909

Surface deposition

The analysis shown in the main text (Fig. 7) is based on the deconvolution of the multimodal distribution revealed in the histogram by multiple Gaussian fits which results is summarized in the Table S7 below.

Table S7. Deconvolution parameters of the multimodal height distribution extracted from Fig. 7.

	Substrate	First layer	Second layer
y_0 (nm ⁻¹)	3.38589E-4 ± 2.10439E-4	3.38589E-4 ± 2.10439E-4	3.38589E-4 ± 2.10439E-4
x_c (nm)	H ₀ = 0.03904 ± 0.01228	H ₁ = 4.79412 ± 0.00783	H ₂ = 9.11519 ± 0.03242
w	2.33446 ± 0.02617	2.12353 ± 0.01656	3.06345 ± 0.0725
A	0.29529 ± 0.00299	0.48913 ± 0.00354	0.20199 ± 0.00418

where each component is described by a Gaussian function:

$$y = y_0 + \frac{A}{w \sqrt{\frac{\pi}{2}}} \cdot \exp\left(-2\left(\frac{x - x_c}{w}\right)^2\right) \quad \text{Eq.S11}$$

Starting from the obtained values, the height of objects has been expressed as the center of the Gaussian distributions (x_c) and the error on that measurement as the half of the full with half maximum (A) of the distributions.

References

- 1 G. M. Sheldrick, *Acta Crystallogr A Found Adv*, 2015, **71**, 3–8.
- 2 G. M. Sheldrick, *Acta Crystallogr C Struct Chem*, 2015, **71**, 3–8.
- 3 D. Nečas and P. Klapetek, *Open Physics*, 2012, **10**, 181–188.